American Mineralogist, Volume 62, pages 990–998, 1977

The crystal structure of deerite

MICHAEL E. FLEET

Department of Geology, University of Western Ontario
London, Ontario, Canada

Abstract

The crystal structure of deerite [$P2_1/a$, a = 10.786(8), b = 18.88(2), c = 9.564(9)A, β = 107.45(5)°] from Panoche, California, has been investigated using intensity data collected with Mo$K\alpha$ radiation on a Picker FACS 1 diffractometer. The structure of the pseudocell with $c' = c/3$ and space group $P2_1/a$ has been determined and refined to a weighted residual index of 0.07. The pseudocell structure has disordered Si and oxygen positions, and there are only three possible ordered arrangements of these: the preferred full structure of deerite has a weighted residual index of 0.08, but it was not possible to refine it. The ideal structural formula is $Fe^{2+}_6Fe^{3+}_3O_3[Si_6O_{17}](OH)_5$, Z = 4. The structure is formed of two structural units continuous along the c-axis direction; (1) a strip of edge-sharing M-atom octahedra, six octahedra in width, oriented parallel to {110}, and (2) a hybrid single-double $[Si_6O_{17}]$ silicate chain. Apical and lateral oxygens of the silicate chain are shared with M octahedra, but the familiar sandwich of tetrahedral–octahedral–tetrahedral coordination polyhedra is not well developed. The basal tetrahedral oxygens enclose a structural void. Fe^{3+} probably occupies the lateral sites in the octahedral strip.

Similar structural units have been reported recently for howieite, which is associated with deerite in rocks of the Franciscan Formation. The arrangement of the silicate chain in chain-silicate structures is constrained by the close-packed oxygen distances in the octahedral strip. This constraint results in a distinctly different structural topology in deerite and howieite compared to pyroxene and amphibole and imparts a characteristic distortion to the silicate chain. In particular, the sides of the six-membered rings in both deerite and howieite are buckled inward.

Introduction

Deerite (along with howieite and zussmanite) occurs in blocks of riebeckite–stilpnomelane schists within metasediments of the Franciscan Formation, California. The type locality is the Laytonville quarry, Mendocino County (Agrell *et al.,* 1965). Deerite has also been reported in stilpnomelane schists, associated with glaucophane schists, in the French and Italian Alps (for example, Agrell and Gay, 1970).

Deerite is a hydrous ferrous, ferric silicate: the proposed formula for a half unit-cell content with (O,OH) = 50 is $(Mg_{0.08}Mn_{0.86}Fe^{2+}_{10.90})_{11.84}(Fe^{3+}_{5.89}Al_{0.38})_{6.27}Si_{11.86}O_{39.95}(OH)_{10.05}$ (Agrell *et al.,* 1967, footnote by Agrell). Agrell *et al.* (1965) report that it is monoclinic, space group $P2_1/a$, with a = 10.755(2), b = 18.870(6), c = 9.568(2)A, β = 107.12(4)°, density 3.837 gm cm^{-3}. It forms black acicular crystals, elongated parallel to c and lozenge-shaped in cross section, with a good {110} cleavage. The crystals are twinned submicroscopically: the twin axis is [001]. More recently, Wenk (1974) has suggested that deerite is in fact orthorhombic, space group *Pnma,* with a = 18.885, b = 3.182 (needle axis), c = 10.337A.

Characteristic Mössbauer spectra and magnetic susceptibility data for deerite have been reported by several laboratories, and the initial interpretations of these data resulted in a certain amount of controversy. Bancroft *et al.,* (1968) interpreted their room-temperature Mössbauer spectrum in terms of three quadrupole doublets: A,A', assigned to Fe^{2+} in sixfold coordination; B,B', assigned to Fe^{3+} in sixfold coordination; C,C', assigned to Fe^{2+} in a distorted fourfold coordination. The fraction of the total Fe content of deerite accommodated in each of the sites, or group of sites, associated with these doublets is approximately 0.47, 0.37, and 0.16, respectively. In a subsequent Mössbauer study, Frank and Bunbury

(1974) confirmed the assignments of the A,A' and B,B' doublets but argued that C,C' should be assigned to Fe^{2+} in sixfold coordination. The Mössbauer spectra show no evidence of low-spin Fe^{2+} and the low magnetic susceptibility data, which Carmichael *et al.* (1966) interpreted to indicate the presence of low-spin Fe^{2+}, is most probably related to antiferromagnetic ordering (Frank and Bunbury, 1974).

The present paper reports on a crystal-structure analysis of deerite. The crystal structures of howieite and zussmanite have been reported recently by Wenk (1974) and Lopes-Vieira and Zussman (1969), respectively. Having spent my undergraduate and graduate years at Manchester during the period when the Deer, Howie and Zussman treatise on mineralogy was being written and produced, I am, to say the least, pleased to participate in completing the basic crystallographic work on this important trio of minerals.

Experimental

The deerite specimen investigated in the present study is from a riebeckite–deerite–garnet schist (No. Pc65), collected as an exotic block in Franciscan rocks near Panoche, San Benito County, California, by Robert M. Wood. Wood (personal communication) reports that the composition of deerite tends to vary within a single hand specimen. Preliminary electron microprobe analyses show that the only appreciable substitution is Mn (3.4 weight percent MnO) for Fe, and since X-ray scattering factors for these two elements are similar, the ideal end-member composition, with a unit-cell content of $Fe^{2+}_{24}\ Fe^{3+}_{12}\ Si_{24}O_{80}(OH)_{20}$, was utilized in the structure analysis.

Deerite crystals are very fragile, since they disrupt readily by parting along the {110} cleavage, and they are ubiquitously twinned. The asterism resulting from crystal disruption combined with the near coincidence of the twin-related reflections renders them very unsuitable for precise X-ray diffraction study. Nevertheless it was possible to remove euhedral acicular crystals from weathered areas of the hand specimen with a minimum of physical damage. Many of these were examined on the precession camera, and one was selected for the collection of intensity data. This was a near-equidimensional crystal bounded by {110} and irregularly terminated along the c axis. Principal dimensions of the crystal were $0.07 \times 0.07 \times 0.03$ mm.

Precession X-ray diffraction films confirmed the observations of Agrell *et al.* (1965) that deerite is monoclinic with space group $P2_1/a$ and is twinned by twofold rotation about [001]. X-ray diffraction patterns are dominated by reflections of the pseudocell with $c' = c/3$ (Fig. 1); of those reflections with $l \neq 3n$, only the pairs $(401, 40\bar{1})$ and $(207, 60\bar{7})$ were observed in the first three levels recorded along the b axis. The twin operation superimposes $hk0$ and $\bar{h}\bar{k}0$ reflections and brings all other pseudocell reflection pairs $(hkl, h'kl)$ with $l = 3n$ and $h' = -(2l/3 + h)$ into near coincidence, the separation of these pairs increasing with decreasing angular distance from the c axis. The maximum observed separation in the $h0l$ plane is 0.71° rotation about the b axis, which is in reasonable agreement with the maximum separation calculated from the unit-cell parameters below (0.52°). The observed variation in the resolution of the twin-related reflection pairs and the fact that the reflections of one twin orientation are somewhat stronger than those of the second orientation allow an unambiguous assignment of monoclinic symmetry. However, if a twinned crystal either somewhat larger than the one investigated, giving more intense reflections, or having a slightly smaller β parameter were examined, the twin-related reflection pairs might not be resolved at all. In this situation the twin axis would appear to be a twofold symmetry axis and the diffraction symmetry of the pseudocell would appear to be orthorhombic. Thus, recalling that the reflections with $l \neq 3n$ are weak and could easily be overlooked, the orthorhombic symmetry and unit-cell data of Wenk (1974) can be accounted for quite readily. The unit-cell parameters for deerite, determined by least-squares refinement of 12 centered reflections measured on a four-circle diffractometer with Zr-filtered Mo$K\alpha$ ($\lambda = 0.7107$A) radiation, are $a = 10.786(8)$, $b = 18.88(2)$, $c = 9.564(9)$A, $\beta = 107.45(5)°$.

X-ray intensity data were collected on a Picker FACS 1 four-circle diffractometer system using a scintillation detector, Zr-filtered Mo$K\alpha$ radiation and

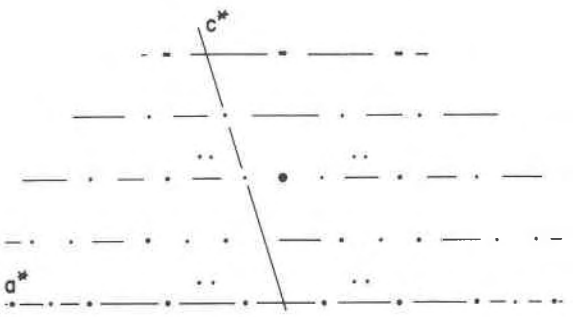

Fig. 1. Sketch of part of zero level, b-axis precession photograph of deerite: Mo$K\alpha$ radiation, $\mu = 30°$, 6-day exposure: lattice rows with $l = 3n$ are lined.

the 2θ scan technique: 40-second stationary background counts, peak-base widths of 2.0° 2θ (uncorrected for dispersion), and a scanning rate of 1.0° per minute. The crystal was mounted on the a^* axis, and all non-equivalent hkl and $hk\bar{l}$ reflections were measured out to $2\theta = 52.5°$. The resulting data were processed by a data-reduction routine which corrected for background, Lorentz, and polarization effects. Standard deviations of structure factors (σ) were calculated from the expression $\sigma = 1/2[1/\mathrm{Lp}.(\sigma_p^2 + \sigma_{b1}^2 + \sigma_{b2}^2 + (0.02I)^2)/I]^{1/2}$, where Lp is the Lorentz-polarization factor, σ_p, σ_{b1}, σ_{b2} are, respectively, the standard deviations for the counting rates of the peak and backgrounds and I is the background-corrected peak intensity. Each reflection whose intensity was less than the associated background plus 3σ was given zero intensity and was rejected in the structure refinement discussed in the following section. It was recognized at an early stage in the work on deerite that the intensity data would not be of high quality. The large mosaic spread of the crystal, due to the combination of asterism and twinning, made crystal alignment difficult. Furthermore, it was not possible to ensure that all of the diffracted intensity of the composite reflections on lattice rows near the c axis was collected in any one 2θ scan. In fact, intensity measurements on the strongest of these reflections ($20\bar{6}$) varied markedly from one crystal alignment to another. Also, peak intensities were relatively weak because the crystal was so small, and there was a dramatic increase in the number of reflections with zero-recorded intensity beyond about 40° 2θ. The final data list contained 3773 reflections. Only 573 reflections had non-zero intensity and of these 515 were pseudocell reflections with $l = 3n$. No correction for absorption was made. However, the crystal was small and fairly equidimensional, and even with $\mu = 74.7$ gm cm^{-1} the absorption corrections were small and not significant, in view of the rather poor quality of the intensity data.

Crystal structure investigation

Space group $P2_1/a$ is uniquely defined by the systematic absences, and hence the crystal structure of deerite must be centrosymmetric. The observed structure factors were converted to normalized structure factors (E's) using program FAME (R. B. K. Dewar, Illinois Institute of Technology, Chicago), and the phases of the 178 reflections with $E \geq 1.5$ were assigned by a reiterative application of Sayre's equation using a modified version of program REL1 (Long, 1965). Sixteen sign combinations for a starting set of seven reflections led to many similar solutions. In the E-map of one of the two solutions with the largest consistency index (0.86) the positions of nine non-equivalent M site atoms, six Si atoms, and several oxygen atoms were recognized. The E-map showed a threefold repetition along the c axis and was clearly dominated by the data for the pseudocell reflections. There were too few reflections with $l \neq 3n$ of non-zero intensity to refine the whole unit cell, and a trial structure based on the E-map information was attempted for the monoclinic pseudocell with $c' = c/3$ and space group $P2_1/a$.

The structure was improved by several stages of full-matrix, least-squares refinement and F_o and F_o–F_c Fourier analysis. The structure refinement was performed with program RFINE (L. Finger, Geophysical Laboratory, Washington). The scattering curves for Fe^0, Si^0, and O^0 were taken from Doyle and Turner (1968), and real and imaginary components of the anomalous dispersion coefficients for Fe^0, Si^0, and Ne^0 were from Cromer (1965). Using reflection data collected out to 39.5° 2θ, the trial structure gave a weighted residual index of 0.34. With improvements suggested by the resulting Fourier analysis and several cycles of refinement, the weighted residual index reduced to 0.14. At this stage it was realized that the two Si positions recognized in the pseudocell have only ⅔ occupancy and that the third Si position with ⅔ occupancy had been mistaken for an oxygen atom. All of the oxygen-atom positions coordinated to M atoms [Fig. 2, equivalent to O(1) to O(18), Table 2] were now defined. The remaining oxygens [equivalent to O(19) to O(25), Table 2], which are the bridging oxygens in the Si tetrahedral chains, have ⅓ occupancy in the pseudocell and were not well-defined on F_o and F_o–F_c maps. In the final stages of refinement the isotropic thermal parameters for these oxygens refined to unrealistic values, and these thermal parameters were arbitrarily fixed at 1.0. The refinement for positional parameters for all atoms (all in general positions) and for isotropic thermal parameters for all but the bridging oxygens converged on values of the conventional and weighted residual indices of 0.095 and 0.072, respectively. Refinement with anisotropic thermal parameters reduced the weighted residual index to 0.065, but the reduction was not significant when tested by the procedure of Hamilton (1965).

When the pseudocell structure is expanded into the true unit cell the atomic positions remaining undefined are those of the atoms which are disordered in the pseudocell structure, Si and bridging oxygens.

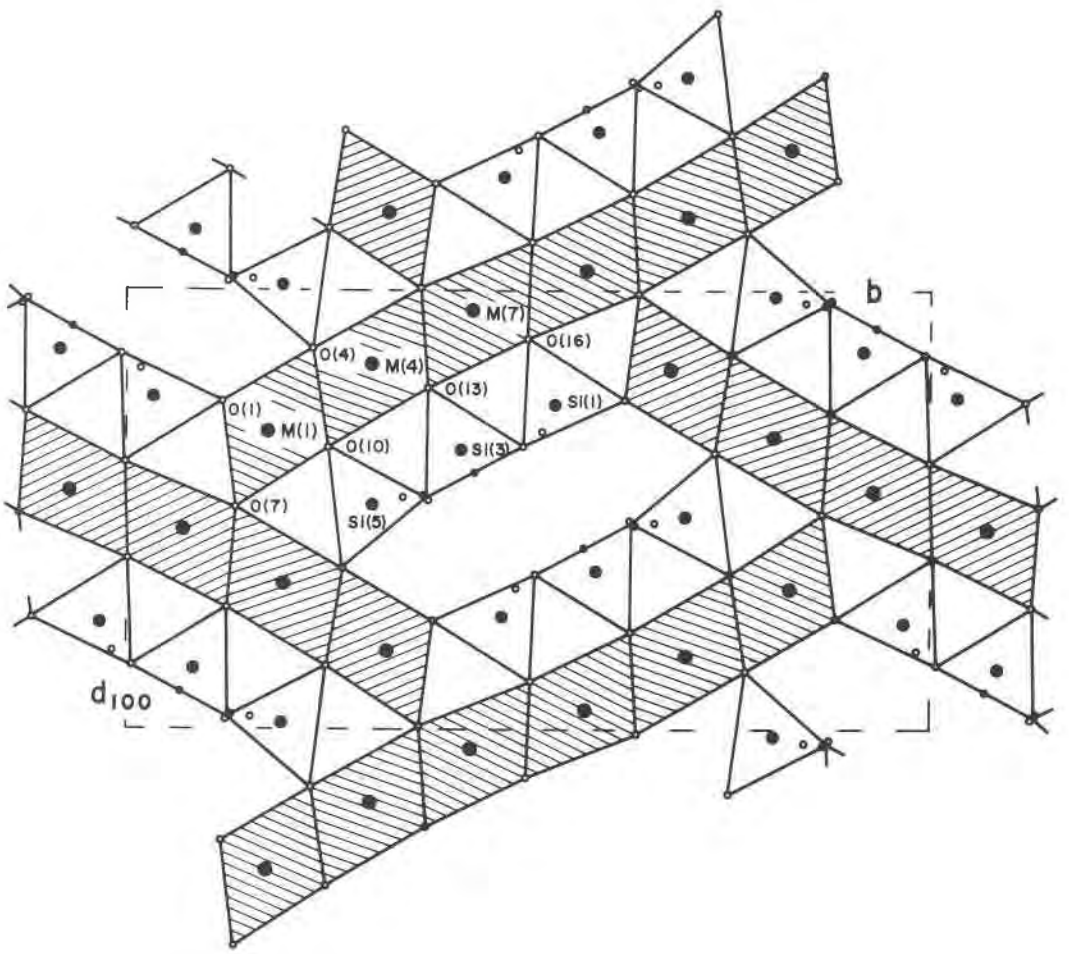

Fig. 2. *c*-axis projection of deerite structure. Each *M* atom and octahedral oxygen represents three superimposed atoms and each Si atom represents two atoms: labels are for lowest of superimposed atoms; bridging tetrahedral oxygens are unlabelled.

Since there were only 58 reflections of the type with $l \neq 3n$ of non-zero intensity, and all of these were either on or marginally above the limit of detectability, it was not expected that the complete deerite structure would be revealed by Fourier synthesis. However, when recognition is taken of reasonable interatomic Si–O, Si–Si, and O–O distances, the only possible arrangement of Si tetrahedra is a $[Si_6O_{17}]$ chain (Fig. 4). As discussed in the following section, the deerite structure is formed of two structural units, an octahedral strip and a silicate chain. There are only three possible arrangements of the silicate chain on the octahedral strip (Fig. 5a), each one related to the other two by translations of the $[Si_6O_{17}]$ chains of $\pm c/3$. Structure factors for these three structures were calculated, and the corresponding weighted residual indices are 0.084, 0.087, and 0.087, respectively. The structure with the lowest residual index also gives better agreement between F_o and F_c for the stronger reflections with $l \neq 3n$ (Table 1) and is assumed to represent the real deerite structure. Furthermore, as discussed in the following section, the back-to-back displacement of the silicate chains for the preferred structure is very similar to that in the structure of the closely-related mineral howieite. Positional and thermal parameters for the full deerite structure are given in Table 2, and observed and calculated structure factors are given in Table 3.[1] Table 3 does not include data for reflections of zero intensity; of these, the numbers within the F_c intervals 0.0 to 49.9, 50.0 to 99.9, 100.0 to 149.9, and 150.0 to 199.9 (normalized to $F_{000} = 2092$) are 2876, 300, 23,

[1] To obtain a copy of this table, order document AM-77-050 from the Business Office, 1909 K Street, N.W., Washington, D. C. 20006. Please remit $1.00 in advance for the microfiche.

Table 1. Observed and calculated structure factors for the three possible deerite structures using reflections with $l \neq 3n$ and intensity greater than background plus 3σ: No. 1 is the preferred deerite structure

hk	F_o	$F_c(1)$	$F_c(2)$	$F_c(3)$
14$\bar{1}$	96	130	142	19
151	92	101	93	13
40$\bar{1}$	93	121	33	83

and 1, respectively, the largest value being 156.5 for 020. As discussed above, there were clearly insufficient non-zero intensity data to refine the full deerite structure. However, the isotropic thermal parameters for the pseudocell are not excessively high, suggesting that the displacements of the pseudocell-related atoms from the ideal positions given in Table 2 would be slight anyway. It should be stressed that the reflections with $l \neq 3n$ were very weak. Being only on or marginally above the limit of detectability, they are particularly susceptible to non-statistical errors (Renninger reflections, and so on), and this is reflected in the increase in weighted residual index from 0.072 for the pseudocell structure to 0.084 for the full deerite structure. Also, the proposed twin mechanism, discussed in the following section, could effect a significant degree of positional disorder between the preferred structure and the other two possible structures and so complicate interpretation of the observed structure-factor data.

Table 2. Positional and isotropic thermal parameters for deerite (all sites are 4*e* equipoint)

Site	x	y	z	B
M(1)	0.3209(5)	0.1756(3)	0.0238(6)	1.1(1)
M(2)	----**	----	0.3572(6)	--
M(3)	----	----	0.6905(6)	--
M(4)	0.1669(5)	0.3042(3)	0.1388(6)	1.1(1)
M(5)	----	----	0.4722(6)	--
M(6)	----	----	0.8055(6)	--
M(7)	0.0443(5)	0.4290(3)	0.2654(6)	1.0(1)
M(8)	----	----	0.5987(6)	--
M(9)	----	----	0.9321(6)	--
Si(1)	0.258(1)	0.5325(8)	0.170(2)	1.4(3)
Si(2)	---	----	0.836(2)	--
Si(3)	0.362(1)	0.4156(8)	0.371(2)	1.1(3)
Si(4)	---	----	0.705(2)	--
Si(5)	0.486(2)	0.3057(9)	0.245(2)	1.6(3)
Si(6)	---	----	0.911(2)	--
O(1)	0.253(2)	0.118(1)	0.164(3)	1.2(4)
O(2)	---	---	0.497(3)	--
O(3)	---	---	0.830(3)	--
O(4)	0.132(2)	0.230(1)	0.298(3)	1.2(4)
O(5)	---	---	0.631(3)	--
O(6)	---	---	0.964(3)	--
O(7)	0.492(2)	0.135(1)	0.080(3)	1.1(4)
O(8)	---	---	0.414(3)	--
O(9)	---	---	0.747(3)	--
O(10)	0.356(2)	0.250(1)	0.203(3)	1.9(5)
O(11)	---	---	0.536(3)	--
O(12)	---	---	0.870(3)	--
O(13)	0.222(2)	0.374(1)	0.323(3)	1.1(4)
O(14)	---	---	0.656(3)	--
O(15)	---	---	0.990(3)	--
O(16)	0.110(2)	0.498(1)	0.122(3)	1.0(4)
O(17)	---	---	0.455(3)	--
O(18)	---	---	0.788(3)	--
O(19)	0.471(6)	0.343(4)	0.083(8)	
O(20)	0.477(6)	0.375(4)	0.346(7)	
O(21)	0.466(6)	0.368(4)	0.801(8)	
O(22)	0.414(5)	0.432(4)	0.551(8)	
O(23)	0.354(6)	0.491(3)	0.775(8)	
O(24)	0.356(6)	0.493(3)	0.303(8)	
O(25)	0.321(6)	0.516(3)	0.023(9)	

** x,y and B parameters indicated by dashes have the same values as those of the immediately preceeding atom

Discussion

Description of the structure

The deerite structure (Fig. 2) has three sets of three virtually equivalent *M* atom positions and six Si positions per asymmetric unit. All the *M* atoms are octahedrally coordinated with oxygen. The *M* octahedra are organized through shared coordination edges into a strip (or band) oriented parallel to {110}, six octahedra in width and continuous along the *c*-axis direction (Fig. 3). The Si tetrahedra form a $[Si_6O_{17}]$ silicate chain (Fig. 4), also continuous along the *c*-axis direction. This is the hybrid single-double silicate chain first reported for howieite (Wenk, 1974). Thus the deerite structure, which has a large unit-cell volume (1858A^3), can be represented rather simply in terms of just two structural units, an *M* octahedral strip and a $[Si_6O_{17}]$ silicate chain. Apical and lateral (non-bridging) tetrahedral oxygens are shared with *M* octahedra. However, the familiar sandwich of tetrahedral–octahedral–tetrahedral coordination polyhedra, found in many chain and sheet silicate structures, is not well developed in deerite (Figs. 2 and 3). Also the interstice enclosed by the basal tetrahedral oxygens is a structural void. The octahedral strips are interconnected by three oxygens [O(7) to O(9)] which are coordinated only to *M* atoms. By analogy with other silicates, the other octahedral oxygens which are not bonded to Si are presumably bonded to H. The H positions, of course, were not resolved in the structure analysis, but the present argument would give five H positions per asymmetric unit, which is in remarkably good agreement with the H content determined earlier by chemical analysis (Agrell *et al.*, 1967).

With all of the H positions occupied, the ratio ferrous/ferric is 1.5. Hence, the actual structural formula of the ideal end-member of deerite is

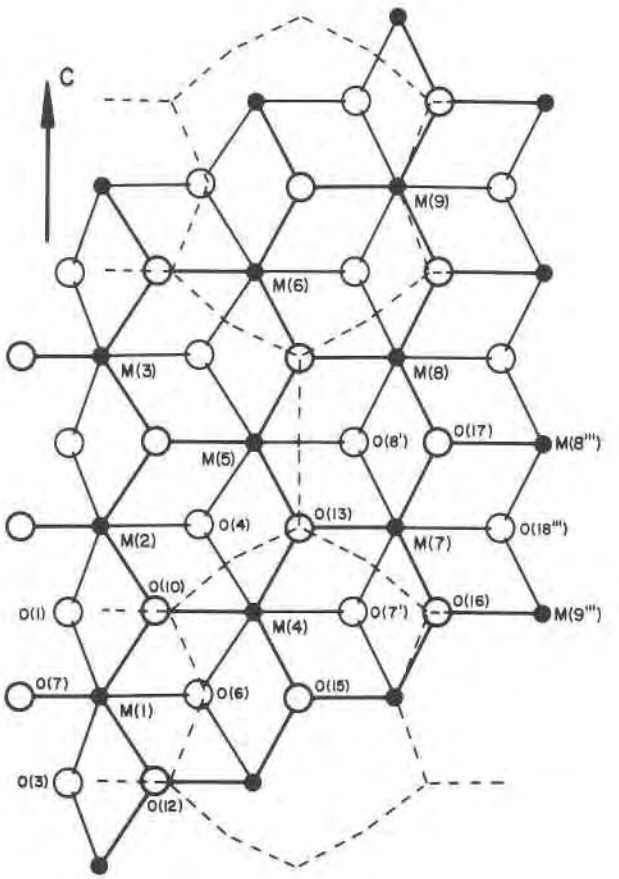

Fig. 3. Part of MO_6 octahedral strip in deerite projected parallel to (110): broken lines indicate position of $[Si_6O_{17}]$ chain above plane of projection.

$Fe_6^{2+}Fe_3^{3+}O_3[Si_6O_{17}](OH)_5$, $Z = 4$. This confirms the estimate of Agrell *et al.* (1967, footnote by Agrell) for the half unit-cell content.

Comparison with other chain silicates

Howieite, which is a hydrous sodium ferrous–ferric silicate, has a crystal structure with analogous structural units to those in deerite; strips of M octahedra, four octahedra in width, enclosed by $[Si_6O_{17}]$ silicate chains (Wenk, 1974). However, all the octahedral oxygen atoms are shared with Si tetrahedra. Thus the octahedral strips and silicate chains form a definite tetrahedral–octahedral–tetrahedral sandwich, and the sandwich units are arranged to give a pseudolayer structure. Also, the interstitial site is occupied by Na, although the back-to-back displacement of the silicate chains (which results in the eightfold-coordinated site for Na) is very similar to that deduced for deerite. Thus deerite and howieite, which are from an unusual medium-grade metamorphic paragenesis, have related crystal structures: the situation is somewhat analogous to the relationship between staurolite and kyanite. Intergrowths of deerite and howieite have been observed (Wood, personal communication), and this can certainly be rationalized on the basis of their structural similarities. One suspects, though, that deerite, by virtue of its greater density and closer structural affinity with the common rock-forming chain silicates, is the higher-grade mineral of the two, and that with increasing metamorphic grade howieite breaks down to deerite and sodium iron amphibole.

The silicate chains in deerite and howieite have quite a different orientation with respect to the M octahedra than in amphibole and pyroxene (Fig. 5). Within an octahedral strip the oxygen atoms are ar-

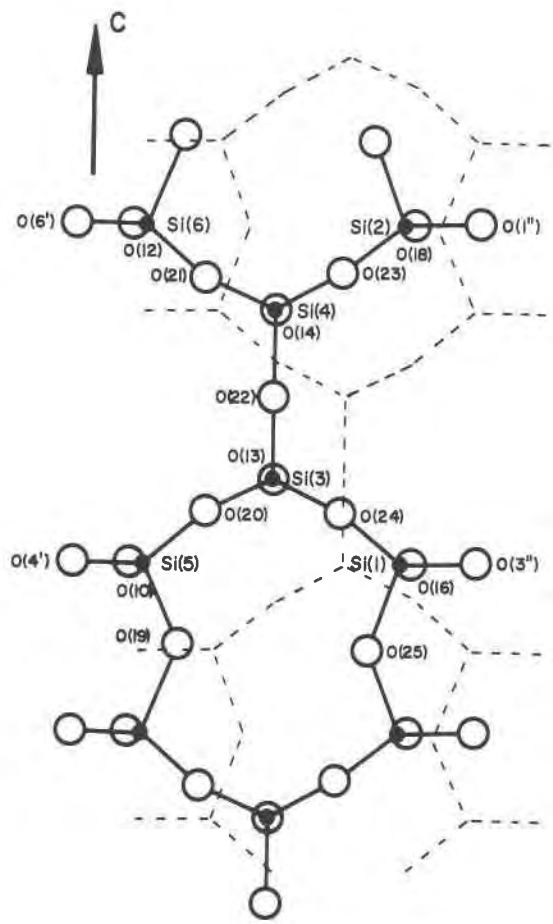

Fig. 4. Part of $[Si_6O_{17}]$ chain in deerite projected parallel to (110) (positioned relative to octahedral strip in Fig. 3): broken lines indicate position of $[Si_6O_{17}]$ chain above plane of projection (the two silicate chains are back-to-back).

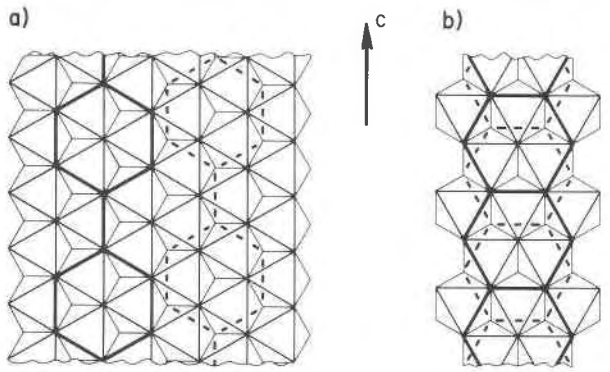

Fig. 5. Relative orientation of silicate chain and MO_6 octahedra in (a) deerite and (b) amphibole: broken lines indicate silicate-chain position on reverse side of octahedral strip. (Note that, for structures with a structural repeat along c axis equivalent to three coordination octahedra, there are three possible chain positions).

ranged in two layers of a hexagonal close-packed array. Adjacent apical oxygens of the associated silicate chains have to be nearest neighbors in the same close-packed layer, and chain orientation is constrained by this requirement. Thus in deerite and howieite the silicate chains are parallel to one of the octahedral edges in the plane of the octahedral strip (Fig. 5a), whereas in amphibole and pyroxene the chains are transverse to one of these edges (Fig. 5b).

Si and M site distortions

Some relevant interatomic distances and bond angles are given in Table 4 (the atom identification labels are consistent with the usage in Figs. 3 and 4; atoms marked by an asterisk are located in adjacent unit cells). The wide variation in the Si–O distances [1.52(7) to 1.83(7)A] is due to the poor resolution of the bridging oxygens in the structure analysis, and this effectively precludes a meaningful analysis of these data. However, most of the distortion in the Si tetrahedra appears to be associated with the structural accommodations required in coupling the silicate chains to the octahedral strips. In particular, the separation of the lateral and apical oxygens is constrained by the nearest-neighbor oxygen distances in the octahedral strip. Thus the bonds to the lateral oxygens must be directed more-or-less normal to the chain direction (Fig. 4), causing the sides of the six-membered tetrahedral rings to be buckled inward: the silicate chain in howieite has a similar distortion. The mean Si–O–Si bond angle (135°) is also somewhat less than the ideal value (141°).

Only data for the average coordination octahedron of each of the groups of three virtually equivalent M atom positions are reported in Table 4. The bond distances and angles for these are quite similar to the corresponding data for howieite. The coordination octahedra of $M(4)$ to $M(6)$ and of $M(7)$ to $M(9)$, which are entirely within the octahedral strip (Fig. 3), each share six octahedral edges. The lateral coordination octahedra, those of $M(1)$ to $M(3)$, share only four octahedral edges. The effect of shared coordination edges in ortho- and chain-silicate structures has been discussed recently by Fleet (1974, 1975). As a result of the electrostatic repulsion between the juxtaposed M atoms, M–M interatomic distances are stretched relative to ideal values. This is accomplished largely by reduction of the related O–M–O bond angles and, in cases where the repulsive forces do not affect all bond distances equally, by stretching of the related M–O bond distances. Thus all of the bond angles associated with shared edges in deerite are markedly less than 90°, and the mean M–O bond distances of the $M(1)$ to $M(3)$ octahedra for bonds associated with two, one, and zero shared edges are 2.17, 2.05, and 1.92A, respectively. Clearly, the principal distortions in the octahedral strip of deerite result from M–M repulsions associated with shared edges, and the overall effect of these, compression perpendicular to the plane of the strip, is exactly the same as that reported for amphibole (Fleet, 1974).

M site occupancies

As discussed above, ideal deerite has six Fe^{2+} and three Fe^{3+} per formula unit. Although it has not been possible to determine the M site occupancies experimentally, it appears likely that Fe^{2+} occupies $M(4)$ to $M(9)$ and Fe^{3+} occupies $M(1)$ to $M(3)$. These site assignments are proposed on stereochemical evidence. The mean M–O distances for $M(4)$ to $M(6)$ and $M(7)$ to $M(9)$ are similar to that expected for Fe^{2+} in octahedral coordination with oxygen (2.17A, Shannon and Prewitt, 1969), and the coordination octahedra of $M(1)$ to $M(3)$ are quite similar to that of $M(2)$ in amphibole, the site that shows consistent enrichment of M^{3+} metals. Furthermore Fe^{3+}, which experiences greater destabilization than Fe^{2+} from shared coordination edges (Fleet, 1974), would be expected to prefer the lateral sites on the octahedral strip, because the coordination octahedra of these sites have fewer shared eges. The mean M–O distance for $M(1)$ to $M(3)$ coordination octahedra *is* somewhat greater than that expected for Fe^{3+} in octahedral coordination with oxygen (1.95A), but much of

Table 4. Interatomic distances and bond angles in deerite

	Distance(Å)		Distance(Å)	Angle(°)
Si(1)-O(3'')	1.62(3)	O(3'')-O(16)	2.68(3)	109(1)
-O(16)	1.66(2)	-O(24)	2.77(7)	120(3)
-O(24)	1.58(6)	-O(25)	2.65(7)	103(2)
-O(25)	1.77(8)	O(16)-O(24)	2.70(6)	113(3)
mean	1.66	-O(25)	2.74(7)	106(2)
		O(24)-O(25)	2.63(10)	104(4)
Si(2)-O(1'')	1.62(3)	O(1'')-O(18)	2.68(3)	109(1)
-O(18)	1.66(2)	-O(23)	2.80(7)	124(3)
-O(23)	1.55(6)	-O(25)*	2.58(7)	101(2)
-O(25)*	1.73(8)	O(18)-O(23)	2.68(6)	113(3)
mean	1.64	-O(25)*	2.70(8)	105(2)
		O(23)-O(25)*	2.54(10)	101(4)
Si(3)-O(13)	1.64(2)	O(13)-O(20)	2.69(6)	115(3)
-O(20)	1.54(6)	-O(22)	2.75(7)	112(2)
-O(22)	1.67(7)	-O(24)	2.71(7)	114(3)
-O(24)	1.60(6)	O(20)-O(22)	2.50(10)	102(3)
mean	1.61	-O(24)	2.56(9)	109(4)
		O(22)-O(24)	2.55(10)	102(3)
Si(4)-O(14)	1.64(2)	O(14)-O(21)	2.59(7)	110(3)
-O(21)	1.52(7)	-O(22)	2.79(7)	110(2)
-O(22)	1.75(7)	-O(23)	2.70(7)	113(3)
-O(23)	1.59(6)	O(21)-O(22)	2.58(10)	104(3)
mean	1.63	-O(23)	2.60(9)	113(4)
		O(22)-O(23)	2.67(9)	106(3)
Si(5)-O(4')	1.65(3)	O(4')-O(10)	2.87(3)	118(1)
-O(10)	1.70(3)	-O(19)	2.66(7)	106(2)
-O(19)	1.67(8)	-O(20)	2.72(7)	111(2)
-O(20)	1.65(7)	O(10)-O(19)	2.62(8)	102(2)
mean	1.67	-O(20)	2.84(7)	116(2)
		O(19)-O(20)	2.58(10)	102(4)
Si(6)-O(6')	1.65(3)	O(6')-O(12)	2.87(3)	118(1)
-O(12)	1.70(3)	-O(19)*	2.72(7)	103(2)
-O(19)*	1.83(7)	-O(21)	2.72(7)	117(3)
-O(21)	1.55(7)	O(12)-O(19)*	2.70(7)	99(2)
mean	1.69	-O(21)	2.70(7)	112(3)
		O(19)*-O(21)	2.71(10)	106(4)

Bridging Oxygen Bond Angles

	Angle(°)		Angle(°)
Si(5)-O(19)-Si(6)*	131(4)	Si(2)-O(23)-Si(4)	138(4)
Si(3)-O(20)-Si(5)	133(4)	Si(1)-O(24)-Si(3)	134(4)
Si(4)-O(21)-Si(6)	142(4)	Si(1)-O(25)-Si(2)*	131(4)
Si(3)-O(22)-Si(4)	138(4)		

	Distance(Å)		Distance(Å)	Angle(°)
M(1)-O(1)	2.02(2)	O(1)-O(3)*	3.188(3)	102(1)
-O(3)*	2.08(2)	-O(6)*	2.88(3)	86.0(9)
-O(6)*	2.20(2)	-O(7)	2.94(3)	96(1)
-O(7)	1.92(2)	-O(10)	+2.71(4)	81(1)
-O(10)	2.16(3)	O(3)*-O(6)*	2.97(3)	87.8(9)
-O(12)*	2.15(3)	-O(7)	2.97(3)	96(1)
mean	2.09	-O(12)*	+2.71(4)	80(1)
-M(2)	3.188(3)	O(6)*-O(10)	+2.80(3)	80.0(8)
-M(3)*	3.188(3)	-O(12)*	+2.84(3)	81.6(8)
-M(4)	3.311(8)	O(7)-O(10)	3.05(4)	96(1)
-M(6)*	3.307(8)	-O(12)*	3.03(4)	96(1)
		O(10)-O(12)*	3.1888(3)	95(1)

*Atoms marked by an asterisk are located in adjacent unit cells
+Indicates shared octahedral coordination edge
Symmetry operations for symmetry related atoms: () x, y, z; (') 1/2+x,1/2-y, z; ('') 1/2-x,1/2+y,-z; (''') -x, -y,-z

Table 4. continued

	Distance(Å)		Distance(Å)	Angle(°)
M(4)-O(4)	2.18(2)	O(4)-O(6)*	3.188(3)	95.8(9)
-O(6)*	2.12(2)	-O(7')	3.34(4)	101.8(9)
-O(7')*	2.13(2)	-O(10)	+2.84(3)	81.1(8)
-O(10)	2.19(2)	-O(13)	+2.86(3)	83.2(9)
-O(13)	2.13(3)	O(6)*-O(7')*	3.31(4)	102.4(9)
-O(15)*	2.15(3)	-O(10)	+2.80(3)	81.0(9)
mean	2.15	-O(15)*	+2.86(3)	84.2(9)
-M(1)	3.311(8)	O(7')*-O(13)	+2.85(3)	83.7(9)
-M(2)	3.307(8)	-O(15)*	+2.86(3)	84.0(9)
-M(5)	3.188(3)	O(10)-O(13)	3.14(4)	93.0(9)
-M(6)*	3.188(3)	-O(15)*	3.15(4)	93.1(9)
-M(7)	3.119(8)	O(13)-O(15)*	3.188(3)	96.2(9)
-M(9)*	3.106(8)			
M(7)-O(7')*	2.08(3)	O(7')*-O(8')*	3.188(3)	101(1)
-O(8')*	2.07(3)	-O(13)	+2.85(3)	86(1)
-O(13)	2.10(2)	-O(16)	+2.78(3)	82(1)
-O(16)	2.16(2)	-O(18''')*	3.22(3)	100.5(9)
-O(17)	2.17(2)	O(8')*-O(13)	+2.86(3)	86.8(9)
-O(18''')*	2.10(2)	-O(17)	+2.78(3)	82(1)
mean	2.11	-O(18''')*	3.22(4)	101.3(9)
-M(4)	3.119(8)	O(13)-O(16)	3.04(4)	91.1(9)
-M(5)	3.106(8)	-O(17)	3.07(3)	92.0(9)
-M(8)	3.188(3)	O(16)-O(17)	3.188(3)	94.9(9)
-M(8''')*	3.25(1)	-O(18''')*	+2.75(4)	80.4(9)
-M(9)*	3.188(3)	O(17)-O(18''')*	+2.78(4)	81.1(9)
-M(9''')*	3.26(1)			

this discrepancy could be explained by stretched M–O distances as a result of uncompensated M–M repulsions.

The present structure analysis partially resolves the controversy in the interpretation of the Mössbauer data for deerite, since there is evidently no fourfold-coordinated Fe^{2+}. The quadrupole doubled B,B' (Bancroft *et al.*, 1968; Frank and Bunbury, 1974) is associated with Fe^{3+} in $M(1)$ to $M(3)$. However, the Mössbauer analysis seems to have very slightly overestimated the proportion of Fe^{3+}. Stereochemically, the two groups of sites $M(4)$ to $M(6)$ and $M(7)$ to $M(9)$ are so similar that one would expect them to produce overlapping Mössbauer peaks for absorption by Fe^{2+}, and this appears to explain the doublet A,A'. The doublet C,C' is more difficult to explain. However, the relative areal extent of A,A' accounts for less than six Fe^{2+} per formula unit, and a tentative explanation for C,C' is that it is attributable to absorption by Fe^{2+} [in a proportion of the $M(4)$ to $M(6)$ sites] which is involved in some electron interaction process with Fe^{3+} in $M(1)$ to $M(3)$, somewhat analogous to the electronic switching proposed for Fe^{2+} and Fe^{3+} in the octahedral site of magnetite (Bauminger *et al.*, 1961).

Crystal morphology and twinning

The arrangement of the structural units parallel to {110} (Fig. 2) readily accounts for the prominence of this form on deerite crystals. The large structural void

and the consequent minimal bonding between the tetrahedral–octahedral–tetrahedral sandwich units explains the fragility of deerite crystals and the ease with which they separate along the {110} cleavage.

Although deerite is dimensionally pseudo-orthorhombic, its structure is not related to that of a hypothetical orthorhombic modification by a slight distortion. Hence the twinning in deerite is probably not due to inversion. However, there must be little difference in free energy between the three possible stacking arrangements of silicate chains and octahedral strips (Fig. 5a), and growth mistakes (which develop into incoherent twin boundaries) could occur very readily. The structural controls on this process are such that the twinned volumes are likely to be one-dimensional domains, continuous along the *c*-axis direction.

Acknowledgments

Thanks go to Robert M. Wood, University of Cambridge, for provision of the deerite sample, for compositional data on deerite in advance of publication, and for several helpful comments. This study was supported by a National Research Council of Canada operating grant.

References

Agrell, S. O. and M. Gay (1970) De la deerite dans les Alpes franco-italiennes. *Bull. Soc. Minéral. Cristallogr., 93,* 263–264.

———, M. G. Bown and D. McKie (1965) Deerite, howieite and zussmanite, three new minerals from the Franciscan of the Laytonville district, Mendocino Co., California (abstr.). *Am. Mineral., 50,* 278.

———, ——— and ——— (1967) Deerite, howieite and zussmanite, three new minerals from the Franciscan of the Laytonville district, Mendocino Co., California (abstr.). *Mineral. Abstracts, 18,* 207.

Bancroft, M. G., R. G. Burns and A. J. Stone (1968) Applications of the Mössbauer effect to silicate mineralogy—II. Iron silicates of unknown and complex crystal structures. *Geochim. Cosmochim. Acta, 32,* 547–559.

Bauminger, R., S. G. Cohen, A. Marinov, S. Ofer and E. Segal (1961) Study of the low-temperature transition in magnetite and the internal fields acting on iron nuclei in some spinel ferrites, using Mössbauer absorption. *Phys. Rev., 122,* 1447–1450.

Carmichael, I. S. E., W. S. Fyfe and D. J. Machin (1966) Low spin ferrous iron in the iron silicate deerite. *Nature, 211,* 1389.

Cromer, D. T. (1965) Anomalous dispersion corrections computed from self-consistent field relativistic Dirac-Slater wave functions. *Acta Crystallogr., 18,* 17–23.

Doyle, P. A. and P. S. Turner (1968) Relativistic Hartree-Fock X-ray and electron scattering factors. *Acta Crystallogr., A24,* 390–397.

Fleet, M. E. (1974) Distortions in the coordination polyhedra of *M* site atoms in olivines, clinopyroxenes and amphiboles. *Am. Mineral., 59,* 1083–1093.

——— (1975) Bond angle distortions in silicate tetrahedra. *Acta Crystallogr., B31,* 1095–1097.

Frank, E. and D. St. P. Bunbury (1974) A study of deerite by the Mössbauer effect. *J. Inorg. Nucl. Chem., 36,* 1725–1730.

Hamilton, W. C. (1965) Significance tests on the crystallographic *R* factor. *Acta Crystallogr., 18,* 502–510.

Long, R. E. (1965) *The Crystal and Molecular Structures of 7,7,8,8,-Tetracyanoquinodimethane and Cyclopropanecarboxamide and a Program for Phase Determination.* Ph. D. Thesis, University of California, Los Angeles.

Lopes-Vieira, A. and J. Zussman (1969) Further detail on the crystal structure of zussmanite. *Mineral. Mag., 37,* 49–59.

Shannon, R. D. and C. T. Prewitt (1969) Effective ionic radii in oxides and fluorides. *Acta Crystallogr., B25,* 925–946.

Wenk, H. R. (1974) Howieite, a new type of chain silicate. *Am. Mineral., 59,* 86–97.

Manuscript received, January 10, 1977; accepted for publication, May 13, 1977.